APPLIED AND ENVIRONMENTAL MICROBIOLOGY, Dec. 1997, p. 4778–4783 Vol. 63, No. 12
0099-2240/97/$04.00+0

In Situ Classification and Image Cytometry of Pelagic Bacteria from a High Mountain Lake (Gossenköllesee, Austria)

JAKOB PERNTHALER,* ALBIN ALFREIDER, THOMAS POSCH, STEFAN ANDREATTA, AND ROLAND PSENNER

Institute of Zoology and Limnology, University of Innsbruck, A-6020 Innsbruck, Austria

Received 3 June 1997/Accepted 26 September 1997

We describe a procedure to measure the cell sizes of pelagic bacteria after determinative hybridization with rRNA-targeted fluorescently labeled oligonucleotide probes. Our approach is based on established image analysis techniques modified for objects simultaneously stained with two fluorescent dyes. It allows the estimation of biomass and cell size distribution and the morphological characterization of different bacterial taxa in plankton samples. The protocol was tested in a study of the bacterioplankton community of a high mountain lake during and after the ice break period. Cells that hybridized with a probe for the domain *Bacteria* accounted for 70% of the bacterial abundance (range, 49 to 83%) as determined by 4′,6′-diamidino-2-phenylindole staining (K. G. Porter and Y. S. Feig, Limnol. Oceanogr. 25:943–948, 1980), but for >85% of the total biomass (range, 78 to 99%). The size distribution for members of the beta subclass of the *Proteobacteria* shifted toward larger cells and clearly distinguished this group from the total bacterial assemblage. In the surface water layer beneath the winter cover, bacteria belonging to the beta 1 subgroup constituted about one-half of the beta subclass abundance. The mean cell volume of the beta 1 subgroup bacteria was significantly less than that of the beta subclass proteobacteria, and the beta 1 subgroup accounted for less than 30% of the total beta subclass biovolume. Two weeks later, the biovolume of the beta *Proteobacteria* had decreased to the level of the beta 1 subgroup, and both the biovolume size distributions and cell morphologies of the beta *Proteobacteria* and the beta 1 subgroup were very similar. We could thus quantify the disappearance of large, morphologically distinct beta subclass proteobacteria which were not members of the beta 1 subgroup during the ice break period. Our results demonstrate that changes in biovolumes and cell size distributions of different bacterial taxa, and eventually of individual populations, reveal hitherto unknown processes within aquatic bacterial assemblages and may open new perspectives for the study of microbial food webs.

Image analysis was introduced into aquatic microbial ecology more than a decade ago to measure the sizes and determine the biovolumes of fluorescently stained bacteria and protists (5, 30). Since then, several substantial improvements in both the image-processing techniques and the hardware have been reported (7, 24–26, 31, 36), and a number of studies have made use of this new approach (6, 9, 13, 17, 21, 27, 32, 34). Increasingly powerful computing facilities and charge-coupled device (CCD) cameras are available to microbial ecologists now, and adequate image analysis software can be obtained, sometimes at no cost (27). Concomitantly, new questions about the ecological regulation of bacterial cell size have successfully been addressed with this technique; these questions include the relationship between bacterioplankton cell size and activity (13, 24) or protistan predation (17, 21, 32), the seasonal and annual variability of bacterial cell volumes (6, 34), and the ranges of bacterial cell sizes and biovolumes in oxic and anoxic layers of lakes (9). Presently, however, size structure analysis of bacterioplankton assemblages can only reveal features which are independent of taxonomic considerations, and there has been no strategy to study in situ the morphological properties, size distributions, and biovolumes of individual bacterial taxa within microbial communities.

One current focus in aquatic microbial ecology is the unknown taxonomic diversity of planktonic bacterial assemblages (14, 16, 20, 28). Fluorescent in situ hybridization with rRNA-targeted oligonucleotide probes (3, 11) is a promising new approach for characterization of pelagic microbial communities. Fluorescent probes have recently been employed to determine the active fraction of marine bacterioplankton (18), to analyze the microbial community structure of lake snow (37) and of the winter cover and plankton of a high mountain lake (1), to demonstrate the importance of members of the beta subclass of the *Proteobacteria* in the bacterioplankton of several oligo- to eutrophic lakes (15), to follow the vertical distribution of members of the delta subclass of the *Proteobacteria* along chemical gradients in a fjord (27), and to monitor major taxonomic shifts in a continuous culture system after the addition of a protistan predator (22, 32). The taxonomic information that has been obtained is still rather general, and the development of probes that specifically characterize individual bacterial populations within pelagic microbial communities is a challenging task for microbial ecologists (4).

Although both methods are based on microscopic evaluation of fluorescently stained objects, only a few studies have combined image analysis cytometry and in situ hybridization of single bacterial cells (19, 38). Ramsing et al. (27) successfully used image analysis to count and determine the sizes of "phy-

* Corresponding author. Present address: Max Planck Institute of Marine Microbiology, Celsiusstrasse 1, D-28359 Bremen, Germany. Phone: 49 421 2028 940. Fax: 49 421 2028 580. E-mail: perntha@mpi-bremen.de.

logenetically stained" (11) bacterioplankton in a fjord, but they did not attempt to perform a detailed morphometric analysis of individual taxonomic groups or to determine cell size distributions. We tried to develop a procedure for measuring the sizes of hybridized bacterial cells from plankton samples based on the improved determinative in situ hybridization technique on membrane filters described by Glöckner et al. (15). Our method should allow workers to simultaneously study and compare the biovolume and cell size distributions of individual bacterial taxa and of the total assemblage. In order to test the applicability of our approach in the field, we followed the biovolume and morphological changes in a major taxonomic group of the bacterioplankton assemblage in a high mountain lake (1) during and after the ice break period.

MATERIALS AND METHODS

Study site and sampling. Gossenköllesee is a small, oligotrophic, high-elevation mountain lake situated in the Tyrolean Alps (2,417 m above sea level; area, 1.7 ha; maximum depth, 9.9 m). It is ice covered for about 8 months a year. For details on the study site see reference 12. On four occasions during late spring to early summer of 1996 (29 May, 13 June, 19 June, and 7 July) we took water samples from the surface and from a depth of 5 m with a Schindler-Patalas sampler. On 29 May the lake was still covered with ice, but the ice disappeared during the first week of June.

In situ hybridization. Fixation for whole-cell in situ hybridization on membrane filters (pore size, 0.2 μm; diameter, 47 mm; Osmonics, Livermore, Calif.) was performed within 1 h after sampling; the procedure of Glöckner et al. (15) was used. Until further processing the filters were stored in small petri dishes in the dark at −20°C. In situ hybridizations of sections from the filters with oligonucleotide probes EUB 338 (for the domain *Bacteria*), BET 42a (for the beta subclass of the *Proteobacteria*), and BONE 663 (for the beta 1 subgroup of the beta subclass of the *Proteobacteria*) (3, 4) were performed as described elsewhere (1, 15, 22). The amino-linked probes were synthesized and conjugated with the indocarbocyanine fluorescent dye Cy3 (Biological Detection System, Pittsburg, Pa.) by MWG Biotech (Munich, Germany). After hybridization, the filter sections were stained with 4′,6′-diamidino-2-phenylindole (DAPI) (final concentration, 1 to 2 $\mu g\ ml^{-1}$) and mounted on microscopic slides in glycerol medium (Citifluor AF 1; Citifluor, Ltd., Canterbury, Great Britain). On some occasions the hybridized and DAPI-stained filter sections were stored overnight at −20°C before embedding, with no apparent loss of fluorescence intensity.

Image acquisition. Image recording was performed by using the image analysis software LUCIA D (version 3.51; Laboratory Imaging, Prague, Czech Republic), a personal computer (with a 486DX processor) equipped with a Matrox IP-8 frame grabber card, and a Peltier cooled CCD video camera (model ZVS-47EC; Optronics Engineering, Goleta, Calif.) mounted on a Zeiss Axioplan microscope (Carl Zeiss, Oberkochen, Germany). The light source for epifluorescent excitation was an Osram type 103 W HBO mercury lamp. The filter sets used were a Zeiss 01 set for UV excitation (DAPI) and a Chroma HQ 41007 set (AF Analysentechnik, Tübingen, Germany) for green excitation (Cy3). Grey images were acquired from microscopic preparations of hybridized filter sections at a magnification of ×102.4 (64× Plan Apochromat objective; additional magnification, ×1.6). The pictures from four screen shots were averaged, and each picture consisted of 524 × 752 pixels with 256 possible grey values per pixel (pixel size, 0.081 μm). We noticed that prior UV excitation caused a strong bleaching of the hybridization signal, so first we recorded a picture under green excitation (Cy3 image), and then we switched filter sets and captured an image from the same microscopic field under UV excitation (DAPI image). DAPI images were recorded at exposure times of 1/60 to 1/8 s, and Cy3 images were recorded at exposure times of 1/4 to 1/2 s. For each hybridized filter section between 15 and 30 pairs of images were recorded.

Image processing. The image analysis software used included a C type macro language, so we composed a program to facilitate the evaluation procedure (available from J.P.). The changing of optical filter sets when we were capturing the image pairs from the same microscopic field often resulted in a small horizontal and vertical discrepancy between the two images (pixel shift), probably due in part to chromatic aberration (27). This could be corrected during the macro execution by using a transparent overlay mode that facilitated the exact alignment of the two images. As the brightness of hybridized cells ranged from overexposed to barely visible, the Cy3 images had to be enhanced by several filtration steps before automated grey-level thresholding for binarization. We used a strategy based on the tophat algorithm (7) and subsequent automatic contrast retransformation to the whole range of grey values (LUCIA function DETECT PEAKS) to separate dim objects from the background. Cell edges were established by convolution with a nonlinear filter based on the "Mexican hat" operator D described by Schröder et al. (29):

$$D' = \begin{bmatrix} -2 & -1 & -1 & -1 & -2 \\ -1 & 2 & 2 & 2 & -1 \\ -1 & 2 & 5 & 2 & -1 \\ -1 & 2 & 2 & 2 & -1 \\ -2 & -1 & -1 & -1 & -2 \end{bmatrix}$$

The image was automatically thresholded at a grey value of 250. Noise was removed from binary images (elimination of single pixels), and object edges were smoothed by morphological opening and subsequent dilatation by 1 pixel. With this procedure, we could usually detect all hybridized cells visible on the original picture, but the binarized objects on the Cy3 image appeared to be larger than the DAPI-stained cells. This had no relevance for the measurements, as the sizes of hybridized cells were determined from the corresponding DAPI images.

Images of DAPI-stained bacteria were preprocessed and binarized as described by Posch et al. (24). All pictures were interactively edited after binarization to eliminate artifacts (e.g., to separate close cells or delete objects of nonbacterial origin). This editing was facilitated by an option that allowed overlay of the binarized picture with either of the two corresponding grey images (Cy3 or DAPI). We also excluded filamentous bacteria if they were only partially within the pictures, because a different image analysis approach is required for appropriate cytometric quantification of such cells (23a). Data acquisition was separated into two steps. First, the macro counted all objects on the DAPI image and measured their pixel areas and perimeters. Next, the two binarized images were combined by a boolean AND operation, and the objects on the resulting image were conditionally dilated or eroded to their original dimensions on the DAPI image. In this way we obtained the fraction of DAPI-stained cells that also showed Cy3 fluorescence. These objects were regarded as hybridized bacteria and counted, and the pixel area and perimeter of each cell was measured. Objects in the Cy3 image that did not match any DAPI-stained cell were regarded either as autofluorescent (e.g., cholorophyll-containing) detritus or nonconjugated grains of fluorescent dye and ignored. Data were stored in MS DOS (Microsoft Corp., Redmond, Wash.) text files and later recalculated by using a macro written in MS Excel. Between 500 and 800 DAPI-stained cells and 100 to 470 hybridized cells were measured per sample, which corresponded to 6 to 13 image pairs.

Total bacterial counts. Portions (100 ml) of subsamples were fixed at the site with a prefiltered formaldehyde solution (final concentration, 2% [wt/vol]), and bacterial cell densities were determined by epifluorescence microscopy as described by Porter and Feig (23).

Calculations, error estimates, and statistical evaluation. The numbers of bacteria that hybridized with different probes were calculated from total bacterial abundance counts and the ratios of hybridized cells to DAPI-stained cells per sample as determined by image analysis. We assumed that the approximate shapes of the bacteria were either spheres or cylinders terminating in hemispheres (13) for calculations of cell dimensions (length, width, and volume) from object pixel areas and perimeters. The biovolumes of DAPI-stained and hybridized bacteria were calculated by determining the products of the abundances and the mean cell volumes. Biovolume size distributions were calculated by splitting up the data logarithmically into eight classes of cell volumes ranging from <0.01 to $>0.64\ \mu m^3$. We pooled all DAPI-stained cells from the three hybridizations and calculated mean cell volumes separately for each size class and date, usually from >100 individual measurements. The biovolume fraction per size class of hybridized bacteria was calculated by determining the product of the relative abundance per size class (percentage of DAPI-stained cells) and the total biovolume present in the size class (21).

To establish the reproducibility and estimate the error range (standard deviations) of our method, four parallel filter sections from a sample collected on 13 June (at the surface) were independently hybridized with probe BONE 663 and processed as described above. The biovolume error range was then estimated from the errors in mean cell volumes and relative abundances of the four parallel samples and the theoretical error for bacterial abundance determination, assuming multiplicative error propagation. The error intervals for the biovolume size distributions for the beta 1 subgroup of the *Proteobacteria* (see Fig. 3b) were calculated (i) from the error ranges of the parallel size distributions, (ii) from the standard deviations of cell volumes per size class, and (iii) from the theoretical error for bacterial abundance determination, assuming multiplicative error propagation.

In order to test if the fluorescent probes interfered with the DAPI signal or if the hybridization process caused a distortion of the original bacterial size distribution (e.g., loss of small cells), we performed reference size measurements with unhybridized cells from formaldehyde-fixed samples obtained on 13 June at the surface and at a depth of 5 m. The bacteria were filtered onto black membrane filters and stained with DAPI (23), and between 800 and 1,000 cells per sample were measured as described previously (24). From a previous study it was known that there is almost no autotrophic picoplankton in Gossenköllesee that could be

TABLE 1. Mean cell volumes of bacterioplankton from Gossenköllesee hybridized with different oligonucleotide probes

Date	Mean cell vol (μm^3)[a]							
	DAPI-stained cells		*Bacteria*[b]		Beta subclass		Beta 1 subgroup	
	Surface	5 m	Surface	5 m	Surface	5 m	Surface	5 m
29 May	0.09 (0.10)	0.06 (0.05)	0.18 (0.17)	0.18 (0.29)	0.25 (0.19)	0.21 (0.24)	0.15 (0.14)	0.14 (0.13)
13 June	0.06 (0.06)	0.06 (0.08)	0.08 (0.08)	0.09 (0.10)	0.14 (0.12)	0.10 (0.06)	0.12 (0.08)	0.13 (0.11)
19 June	0.07 (0.10)	0.08 (0.08)	0.08 (0.12)	0.09 (0.12)	0.13 (0.13)	0.11 (0.08)	0.13 (0.08)	0.14 (0.10)
7 July	0.08 (0.10)	0.08 (0.10)	0.10 (0.14)	0.10 (0.13)	0.15 (0.15)	0.16 (0.15)	0.13 (0.08)	0.15 (0.10)

[a] The numbers in parentheses are standard deviations.
[b] Cells stained with EUB 338.

confused with hybridized bacteria (1). This was occasionally verified by inspecting unhybridized DAPI-stained samples under green excitation.

The statistical analysis was carried out by using the software package STATISTICA 4.5 (Stat-Soft Inc., Tulsa, Okla.). We tested for differences in mean cell volumes by using three factorial analyses of variance (staining type, sampling date, and sampling depth) and post hoc comparisons (Scheffé tests). The following hypotheses were evaluated: (i) the mean cell volumes of bacteria hybridizing with EUB 338 are different from the mean cell volumes of the total community (all DAPI-stained cells), and this difference is affected by sampling date and depth (i.e., there are significant first-order interactions); (ii) the mean cell volumes of cells hybridizing with EUB 338 and BET 42a are different, and this difference is affected by sampling time and date; and (iii) the mean cell volumes of cells hybridizing with BET 42a and BONE 663 are significantly different before the ice break, but not after.

RESULTS

Mean cell volumes. The mean cell volumes of DAPI-stained and hybridized bacterial cells varied both between the sampling dates and at the two depths (Table 1). A three-factorial analysis of variance revealed significant differences ($n = 2964$; $F = 218$; $P < 0.001$) in the mean cell volumes of all DAPI-stained bacteria and cells that hybridized with EUB 338, and these differences were affected by the sampling date ($F = 58$; $P < 0.001$), but not by sampling depth. The cell volumes of members of the *Bacteria* and the beta subclass of the *Proteobacteria* were significantly different ($n = 1,240$; $F = 63$; $P < 0.001$), and there were first-order interactions with both sampling depth ($F = 4$; $P < 0.05$) and date ($F = 85$; $P < 0.001$). A post hoc comparison of the cell volumes of members of the beta subclass and beta 1 subgroup of the *Proteobacteria* revealed significant differences only on 29 May at the surface ($n = 107$; $P < 0.005$).

Biovolumes. The total bacterial biovolume ranged from 1.9×10^4 to 3.4×10^4 μm^3 ml^{-1} and was greatest before the ice break (Fig. 1). The fraction of bacteria that could be detected with fluorescent probe EUB 338 was between 49 and 83% of the total abundance (data not shown), but this fraction accounted for between 79 and 99% of the total biovolume. At the surface the biovolume of members of the beta subclass of the *Proteobacteria* dropped from 2.2×10^4 to 0.9×10^4 μm^3 ml^{-1} during the ice break period and increased again on the last sampling date. A similar but less pronounced pattern was found at a depth of 5 m. Beta *Proteobacteria* accounted for between 42 and 90% of the bacterial biovolume that could be detected with fluorescent probes (i.e., the EUB 338-positive bacterial biovolume). The biovolume of bacteria hybridizing with BONE 663 was less variable; it ranged from 0.57×10^4 to 1.1×10^4 μm^3 ml^{-1}. On 29 May at the surface the members of the beta 1 subgroup accounted for only 29% of the biovolume of the beta *Proteobacteria*, but they accounted for 78% after the ice break period (13 June).

Size distributions and cell morphology. The size distribution of the total bacterial assemblage was bimodal and shifted toward smaller cells after the ice break period (Fig. 2). The peak consisting of DAPI-stained cells with volumes of 0.08 to 0.16 μm^3 could be assigned to members of the beta subclass of the *Proteobacteria*, which were distributed predominantly in the larger size classes. At the first sampling, small cells (volume, 0.01 to 0.04 μm^3) were only partially detected by fluorescent probe EUB 338, yet the same bacterial size fraction could be readily visualized by hybridization on the later dates (Fig. 2). These cells did not belong to the beta subclass of the *Proteobacteria*, and we did not attempt to classify them with other fluorescent probes.

At the first and last sampling dates the beta subclass proteobacteria accounted for the major part of the total probe-detectable biovolume in the larger (>0.08-μm^3) cell size classes (data not shown). During the ice break period a drastic

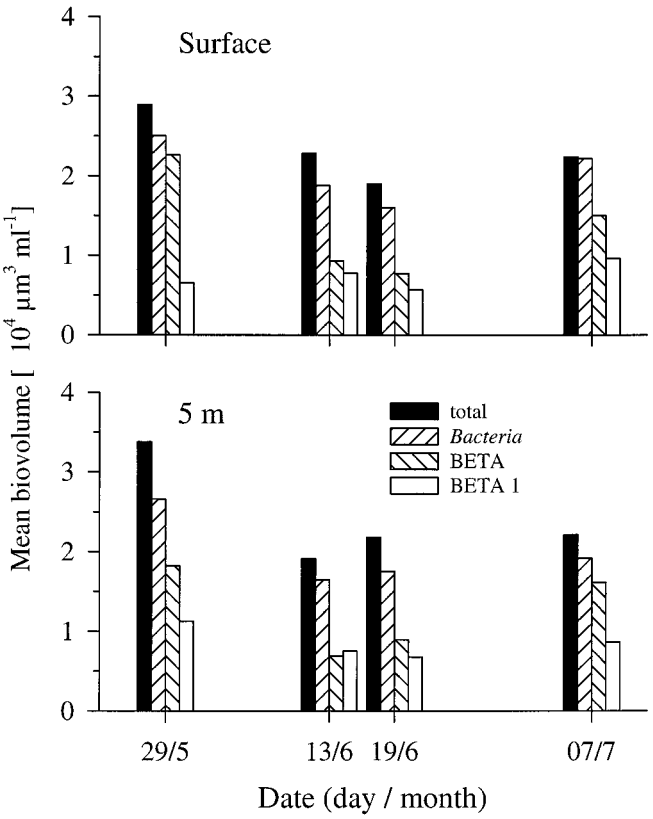

FIG. 1. Mean biovolumes of the total bacterial assemblage in Gossenköllesee and of cells hybridized with different fluorescent probes. *Bacteria*, cells stained with probe EUB 338; BETA, beta subclass of the *Proteobacteria*; BETA 1, beta 1 subgroup of the beta *Proteobacteria*. Samples were obtained from the surface and from a depth of 5 m.

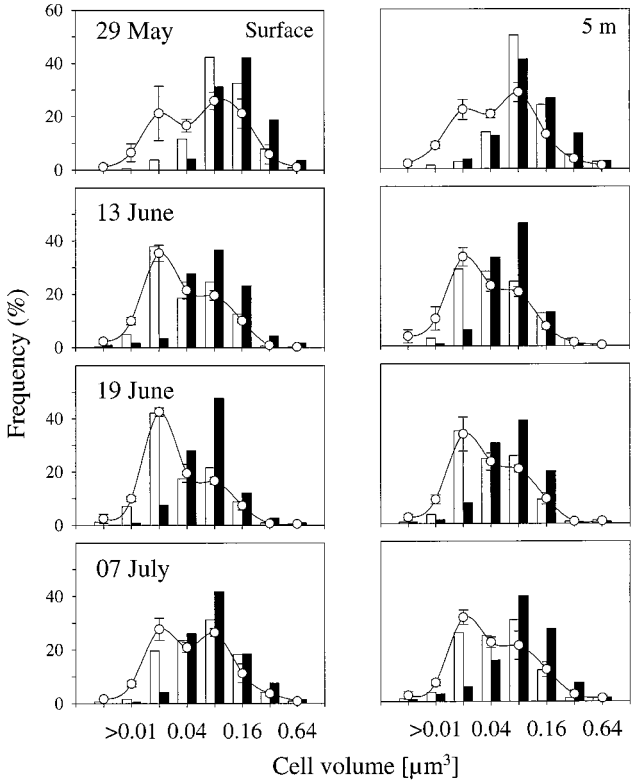

FIG. 2. Cell volume size distributions of the microbial assemblage in Gossenköllesee and of cells hybridized with different fluorescent probes. The error bars indicate the ranges from three replicate size distributions per sample. Open bars, *Bacteria*; solid bars, beta subclass of the *Proteobacteria*; ○, DAPI-stained cells. Samples were obtained from the surface and from a depth of 5 m.

decrease in biovolume in the larger cell size fractions (0.16 to 0.64 μm^3) of the beta *Proteobacteria* was observed in the surface water samples, whereas the biovolume fraction accounted for by the members of the beta 1 subgroup was largely unaffected (Fig. 3a and b). In order to visualize morphological changes, we depicted cell volume and cell length distributions as contour plots of two-dimensional histograms (Fig. 3c through f). Generally, the beta subclass of the *Proteobacteria* decreased in cell volume during the ice break period (Table 1), and there was a shift toward more elongated cells (Fig. 3c and d). The beta *Proteobacteria* with cell volumes between 0.04 and 0.08 μm^3 increased in cell length by almost 30% during the ice break period, and these organisms morphologically closely resembled the members of the beta 1 subgroup on 13 June (Fig. 3e and f). The cell volume distribution of the beta 1 subgroup remained virtually unaltered, but again we observed an increase in the proportion of elongated cells on 13 June.

Error estimates. The biovolume of members of the beta 1 subgroup of the *Proteobacteria* from four parallel hybridizations was $0.78 \times 10^4 \pm 0.21 \times 10^4$ μm^3 ml^{-1} (mean ± standard deviation) (Fig. 1). The total scatter of the biovolume size distributions for replicate hybridizations with probe BONE 663 (minima to maxima) ranged from less than ±1 to ±5% per size class (Table 2). A comparison of the size distributions of hybridized and unhybridized bacteria on 13 June showed that most deviations between the data obtained with the two approaches fell within the range of the replicates, from <0.5% to a maximum of 7% per size class.

DISCUSSION

Image analysis. We tried to adapt an image analysis system that has been used successfully in several studies of microbial ecology (1, 12, 21, 24, 32, 34) for a new set of questions. Bacterial cell sizes have been accurately measured by using very different software, thresholding procedures, and hardware (6, 7, 9, 17, 27, 31), and details of the preprocessing strategies and the level of automation of our image analysis system have been presented elsewhere (24). Below, we discuss some essential hardware and software prerequisites, as well as the difficulties of measuring sizes of hybridized bacterioplankton that have to be addressed irrespective of the image analysis equipment.

Fluorescent staining protocols may influence the apparent size of bacterial cells. Suzuki et al. (35) observed a significant difference in mean cell volumes of marine bacterioplankton cells stained with DAPI or acridine orange, a fluorescent dye that labels both DNA and RNA (39). Brightly hybridized bacteria in our samples usually appeared to be larger than their DAPI images (23a), which may have been due to the absolute amounts of DNA and rRNA per cell and also to the localization of the two nucleic acids within the bacterium (10). The key strategy of our approach was therefore the indirect size mea-

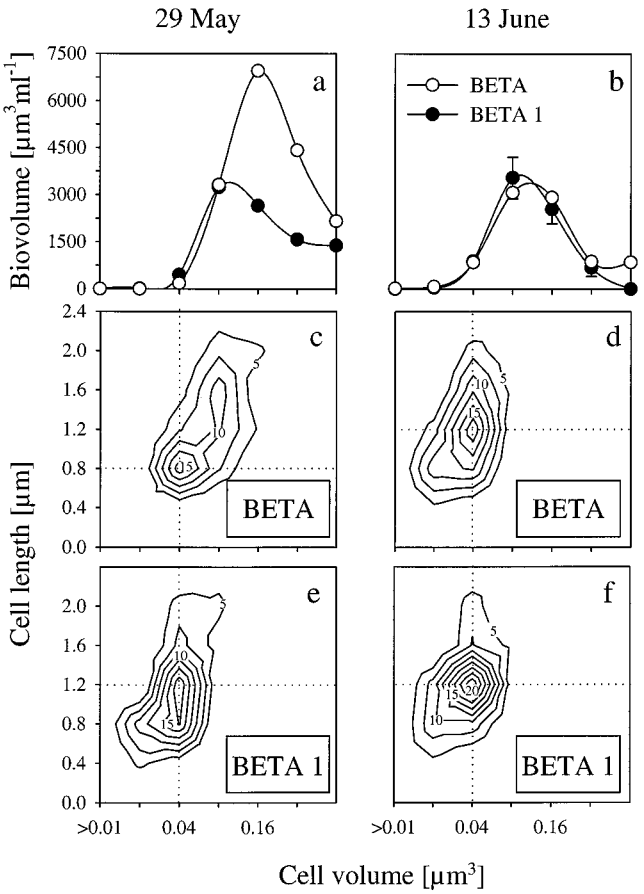

FIG. 3. (a and b) Biovolume size distributions for members of the beta subclass and beta 1 subgroup of the *Proteobacteria* obtained from the surface before and after the ice break period. (c through f) Contour plots of cell volume versus cell length distribution for the two groups for the same period. The numbers on the contour lines are frequencies (expressed as percentages). BETA, beta subclass of the *Proteobacteria*; BETA 1, beta 1 subgroup of the beta *Proteobacteria*.

TABLE 2. Size distributions and error ranges for cells hybridized with probe BONE 663 from four parallel samples and for DAPI-stained cells on 13 June as determined by the standard image analysis protocol (prehybridized) and after the hybridization procedure (hybridized)

Cell vol (μm^3)	%[a] in:				
	BONE 663 surface samples	DAPI-stained surface samples		DAPI-stained 5-m samples	
		Prehybridized	Hybridized	Prehybridized	Hybridized
<0.01	0	6	3 (±1)	6	4 (±2)
0.01–0.02	0	7	10 (±1)	9	10 (±4)
0.02–0.04	3 (±2)	37	34 (±4)	35	33 (±3)
0.04–0.08	23 (±3)	16	21 (±3)	16	23 (±2)
0.08–0.16	54 (±5)	18	21 (±4)	22	20 (±2)
0.16–0.32	17 (±5)	10	10 (±1)	9	7 (±1)
0.32–0.64	3 (±2)	3	1 (±1)	3	1 (±1)
>0.64	0	3	0	1	0

[a] The values in parentheses indicate the ranges obtained from replicate measurements (for the surface samples $n = 6$, and for the 5-m samples $n = 3$).

surement of hybridized bacterial cells from a standard fluorescent staining procedure (with DAPI) (13), because our image analysis procedure was size calibrated by using latex beads with fluorescent properties similar to those of DAPI-stained bacteria (24–26). Moreover, the Cy3 hybridization signal tended to fade more rapidly than the DAPI fluorescence, which probably influenced apparent cell dimensions if they were determined directly from hybridized bacteria. We also observed that the Cy3 fluorescence of individual hybridized bacteria strongly differed in intensity, and such differences have been attributed to the rather variable ribosome contents of individual bacteria in natural communities (4). Finally, determining the cell sizes of a hybridized bacterial population from DAPI images facilitates the positioning of the population within the size distribution of the total assemblage, provided that the hybridization does not introduce a systematic bias. We could show that this was not the case in our samples (Table 2), yet there are numerous sources of error that have to be considered when the size distributions of hybridized bacteria are compared, such as a nonrandom distribution of cells on the filters, differences between repeated hybridizations or DAPI stainings, operator selectivity when acquiring or editing images, and systematic errors of the image analysis procedure. However, the empirically determined error from parallel samples (Table 2; Fig. 3b) shows that we could determine both the cell sizes and biovolumes of hybridized bacteria within a clearly confined range of precision. We chose bacteria hybridizing with probe BONE 663 for error estimates because we expected the greatest variability among the replicates. Members of the beta 1 subgroup of the *Proteobacteria* usually accounted for less than 20% of all DAPI-stained objects, whereas much larger proportions hybridized with the other two probes, and thus the smallest number of individual cells was measured in BONE 663-stained samples (103 to 147 cells per sample; with EUB 338, 225 to 467 cells per sample were measured).

An essential piece of hardware for the measurement of hybridized bacteria is a camera which can be easily adapted to a wide range of fluorescence intensities. Our CCD camera covers an illumination range from 0.005 to >32.000 lx and permits flexible adjustment of shutter speed, contrast, and brightness. However, a pixel shift between DAPI and Cy3 images of the same microscopic field could not be avoided with our microscopic setup, even if great care was taken not to cause vibrations when filter sets were changed. Thus, it was important that our software had a powerful image alignment facility. A macro that combined interactive and automated steps proved to be very valuable, because it sped up evaluation and moreover allowed the processing to be performed by operators with little knowledge about image analysis.

Biovolume and size structure of hybridized lake bacteria. A high percentage (up to 83%) of the bacterioplankton in Gossenköllesee could be visualized with eubacterial probe EUB 338 (1), and the mean cell volume of probe-detectable bacteria was significantly greater than the mean cell volume of the whole assemblage (Table 1). As a consequence, almost all bacterial biovolume was accounted for by determinative fluorescent probing (Fig. 1), which is strong support for the relevance of the in situ hybridization technique in studies of aquatic microbial ecology. However, after the ice break period we could also detect the majority of small bacteria in the size range from 0.02 to 0.04 μm^3 with EUB 338 (Fig. 2). Therefore, cell size does not seem to impede the hybridization approach, although our study was certainly facilitated by the relatively large mean cell size of the bacterioplankton in the high mountain lake studied (Table 1). The fraction of small probe-detectable cells that did not hybridize with probe BET 42a was negligible on the first sampling date, but these organisms accounted for >40% of the total assemblage after the ice break (Fig. 2). Presently we cannot taxonomically position these bacteria, yet they could clearly be distinguished morphologically from the beta subclass proteobacteria by their cell volume distributions (Fig. 2).

The biovolume fluctuations observed in the total bacterial assemblage were much less pronounced than those observed in the beta subclass of the *Proteobacteria* (Fig. 1). The changes in the biovolume size distribution (Fig. 3a and b), as well as the morphological transformation (Fig. 3c and d) of bacteria from this taxonomic group, suggest that a class of large rod-shaped beta subclass proteobacteria with cell volumes between 0.16 and 0.64 μm^3 disappeared during the ice break period. It is also clear that these organisms did not belong to the beta 1 subgroup of the *Proteobacteria*. At this stage, we can only speculate about the reasons for such major biovolume shifts in the bacterioplankton of Gossenköllesee, as an investigation of the underlying ecological processes was beyond the scope of our study. Still, our results demonstrate that even at the level of large taxonomic entities, such as subgroups of the *Proteobacteria*, we may encounter important transformations in bacterial assemblages that cannot be revealed by any other means (22, 32).

Both mean size and cell size distributions have been used to elucidate the growth and cell cycles of laboratory bacterial populations (10). Oligonucleotide probes that specifically stain individual bacterial strains (species) combined with image analysis cytometry might thus help workers analyze the in situ growth patterns of single microbial populations (e.g., in the context of size-dependent mortality rates) (32, 33). Such specific probes have already been designed for bacteria from other systems (2, 8; for a review see reference 4), and we hope that our approach will attract microbial ecologists to the study of bacterial "life histories."

ACKNOWLEDGMENTS

We thank Birgit Sattler, who stood by us even on very thin ice, and Rudolf Amann, Frank-Oliver Glöckner, and Ruben Sommaruga for constructive criticism.

J.P. and A.A. were financed by a grant from the Fonds zur Förderung der wissenschaftlichen Forschung (project P-10184-MOB awarded to R.P.).

REFERENCES

1. **Alfreider, A., J. Pernthaler, R. Amann, B. Sattler, F. O. Glöckner, A. Wille, and R. Psenner.** 1996. Community analysis of the bacterial assemblages in the winter cover and pelagic layers of a high mountain lake using in situ hybridization. Appl. Environ. Microbiol. **62:**2138–2144.
2. **Amann, R., J. Snaidr, M. Wagner, W. Ludwig, and K.-H. Schleifer.** 1996. In situ visualization of high genetic diversity in a natural microbial community. J. Bacteriol. **178:**3496–3500.
3. **Amann, R. I., L. Krumholz, and D. A. Stahl.** 1990. Fluorescent oligonucleotide probing of whole cells for determinative, phylogenetic, and environmental studies in microbiology. J. Bacteriol. **172:**762–770.
4. **Amann, R. I., W. Ludwig, and K.-H. Schleifer.** 1995. Phylogenetic identification and in situ detection of individual microbial cells without cultivation. Microbiol. Rev. **59:**143–169.
5. **Bjørnsen, P. K.** 1986. Automatic determination of bacterioplankton biomass by image analysis. Appl. Environ. Microbiol. **51:**1199–1204.
6. **Bjørnsen, P. K., B. Riemann, J. Pock-Steen, T. G. Nielsen, and S. J. Horsted.** 1989. Regulation of bacterioplankton production and cell volume in a eutrophic estuary. Appl. Environ. Microbiol. **55:**1512–1518.
7. **Bloem, J., M. Veninga, and J. Shepherd.** 1995. Fully automatic detection of soil bacterium numbers, cell volumes, and frequencies of dividing cells by confocal laser scanning microscopy and image analysis. Appl. Environ. Microbiol. **61:**926–936.
8. **Boyle, M., T. Ahl, and S. Molin.** 1995. Application of a strain-specific rRNA oligonucleotide probe targeting *Pseudomonas fluorescens* Ag1 in a mesocosm study of bacterial release into the environment. Appl. Environ. Microbiol. **61:**1384–1390.
9. **Cole, J. J., M. L. Pace, N. F. Caraco, and G. S. Steinhart.** 1993. Bacterial biomass and cell size distribution in lakes: more and larger cells in anoxic waters. Limnol. Oceanogr. **38:**1627–1632.
10. **Cooper, S.** 1991. Bacterial growth and division. Biochemistry and regulation of procaryotic and eucaryotic division cycles. Academic Press, Harcourt, Brace & Co., Publishers, San Diego, Calif.
11. **DeLong, E. F., G. S. Wickham, and N. R. Pace.** 1989. Phylogenetic strains: ribosomal RNA-based probes for the identification of single cells. Science **143:**1360–1363.
12. **Felip, M., B. Sattler, R. Psenner, and J. Catalan.** 1995. Highly active microbial communities in the ice and snow cover of a high mountain lake. Appl. Environ. Microbiol. **61:**2394–2401.
13. **Gasol, J. M., P. A. delGiorgio, R. Massana, and C. M. Duarte.** 1995. Active versus inactive bacteria: size-dependence in a coastal marine plankton community. Mar. Ecol. Prog. Ser. **128:**91–97.
14. **Giovannoni, S. J., T. B. Britschgi, C. L. Moyer, and K. G. Field.** 1990. Genetic diversity in Sargasso Sea bacterioplankton. Nature **345:**60–63.
15. **Glöckner, F. O., R. Amann, A. Alfreider, J. Pernthaler, R. Psenner, K. H. Trebesius, and K. H. Schleifer.** 1996. An in situ hybridization protocol for detection and identification of planktonic bacteria. Syst. Appl. Microbiol. **19:**403–406.
16. **Höfle, M. G., and I. Brettar.** 1996. Genotyping of heterotrophic bacteria from the central Baltic Sea by use of low-molecular-weight RNA profiles. Appl. Environ. Microbiol. **62:**1383–1390.
17. **Jürgens, K., and H. Güde.** 1994. The potential impact of grazing-resistant bacteria in planktonic systems. Mar. Ecol. Prog. Ser. **112:**169–188.
18. **Karner, M., and J. A. Fuhrman.** 1997. Determination of active marine bacterioplankton: a comparison of universal 16S rRNA probes, autoradiography, and nucleoid staining. Appl. Environ. Microbiol. **63:**1208–1213.
19. **Møller, S., C. S. Kristensen, L. K. Poulsen, J. M. Carstensen, and S. Molin.** 1995. Bacterial growth on surfaces: automated image analysis for quantification of growth rate-related parameters. Appl. Environ. Microbiol. **61:**741–748.
20. **Muyzer, G., E. C. de Waal, and A. G. Uitterlinden.** 1993. Profiling of complex microbial populations by denaturing gradient gel electrophoresis analysis of polymerase chain reaction-amplified genes coding for 16S rRNA. Appl. Environ. Microbiol. **59:**695–700.
21. **Pernthaler, J., B. Sattler, K. Šimek, A. Schwarzenbacher, and R. Psenner.** 1996. Top-down effects on the size-biomass distribution of a freshwater bacterioplankton community. Aquat. Microb. Ecol. **10:**255–263.
22. **Pernthaler, J., T. Posch, K. Šimek, J. Vrba, R. Amann, and R. Psenner.** 1997. Contrasting bacterial strategies to coexist with a protistan predator. Appl. Environ. Microbiol. **63:**596–601.
23. **Porter, K. G., and Y. S. Feig.** 1980. The use of DAPI for identifying and counting aquatic microflora. Limnol. Oceanogr. **25:**943–948.

23a. **Posch, T.** Unpublished data.

24. **Posch, T., J. Pernthaler, A. Alfreider, and R. Psenner.** 1997. Cell-specific respiratory activity of aquatic bacteria studied with the tetrazolium reduction method, Cyto-Clear slides, and image analysis. Appl. Environ. Microbiol. **63:**867–873.
25. **Psenner, R.** 1991. Determination of bacterial cell volumes by image analysis. Verh. Int. Ver. Limnol. **24:**2605–2608.
26. **Psenner, R.** 1993. Determination of size and morphology of aquatic bacteria by automated image analysis, p. 339–345. *In* P. Kemp, B. F. Sherr, E. B. Sherr, and J. Cole (ed.), Handbook of methods in aquatic microbial ecology. Lewis Publishers, Boca Raton, Fla.
27. **Ramsing, N. B., H. Fossing, T. G. Ferdelman, F. Andersen, and B. Thamdrup.** 1996. Distribution of bacterial populations in a stratified fjord (Mariager Fjord, Denmark) quantified by in situ hybridization and related to chemical gradients in the water column. Appl. Environ. Microbiol. **62:**1391–1404.
28. **Schmidt, T. M., E. F. DeLong, and N. R. Pace.** 1991. Analysis of a marine picoplankton community by 16S rRNA gene cloning and sequencing. J. Bacteriol. **173:**4371–4378.
29. **Schröder, D., C. Krambeck, and H. J. Krambeck.** 1990. Einflüsse digitaler Bildsegmentierungstechniken auf die quantitative Analyse fluoreszierenden mikrobiellen Planktons, p. 827–836. *In* W. Pillmann and A. Jaeschke (ed.), Informatik für den Umweltschutz. Springer Verlag, Berlin, Germany.
30. **Sieracki, M. E., P. W. Johnson, and J. M. Sieburth.** 1985. Detection, enumeration, and sizing of planktonic bacteria by image-analyzed epifluorescent microscopy. Appl. Environ. Microbiol. **49:**799–810.
31. **Sieracki, M. E., S. E. Reichenbach, and K. L. Webb.** 1989. Evaluation of automated threshold selection methods for accurately sizing microscopic fluorescent cells by image analysis. Appl. Environ. Microbiol. **55:**2762–2772.
32. **Šimek, K., and T. H. Chrzanowski.** 1992. Direct and indirect evidence of size-selective grazing on pelagic bacteria by freshwater nanoflagellates. Appl. Environ. Microbiol. **58:**3715–3720.
33. **Šimek, K., J. Vrba, J. Pernthaler, T. Posch, P. Hartmann, J. Nedoma, and R. Psenner.** 1997. Morphological and compositional shifts in an experimental bacterial community influenced by protists with contrasting feeding modes. Appl. Environ. Microbiol. **63:**587–595.
34. **Sommaruga, R., and R. Psenner.** 1995. Permanent presence of grazing-resistant bacteria in a hypertrophic lake. Appl. Environ. Microbiol. **61:**3457–3459.
35. **Suzuki, M., E. B. Sherr, and B. F. Sherr.** 1993. DAPI direct counting underestimates bacterial abundances and average cell size compared to AO direct counting. Limnol. Oceanogr. **38:**1566–1570.
36. **Viles, C. L., and M. E. Sieracki.** 1992. Measurement of marine picoplankton cell size by using a cooled charge-coupled device camera with image-analyzed fluorescent microscopy. Appl. Environ. Microbiol. **58:**584–592.
37. **Weiss, P., B. Schweitzer, R. Amann, and M. Simon.** 1996. Identification in situ and dynamics of bacteria on limnetic organic aggregates (lake snow). Appl. Environ. Microbiol. **62:**1998–2005.
38. **Whiteley, A. S., A. G. O'Donnell, S. J. Macnaughton, and M. R. Barer.** 1996. Cytochemical colocalization and quantitation of phenotypic and genotypic characteristics in individual bacterial cells. Appl. Environ. Microbiol. **62:**1873–1879.
39. **Zelenin, A. V.** 1993. Acridine orange as a probe for molecular and cell biology, p. 83–99. *In* W. T. Mason (ed.), Fluorescent and luminescent probes for biological activity. A practical guide for quantitative real-time analysis. Academic Press, Harcourt, Brace & Co., Publishers, London, United Kingdom.